Available online at www.sciencedirect.com
ScienceDirect
Trans. Nonferrous Met. Soc. China 33(2023) 2449−2460
Transactions of Nonferrous Metals Society of China
www.tnmsc.cn

Formation of ductile close-packed hexagonal solid solution on improving shear strength of Au−Ge/Cu soldering joint

Meng WANG[1,2], Jian PENG[1]

1. School of Materials Science and Engineering, Central South University, Changsha 410083, China;
2. Aragón Nanoscience and Materials Institute (CSIC−University of Zaragoza) and Condensed Matter Physics Department, C/Pedro Cerbuna 12, 50009 Zaragoza, Spain

Received 24 April 2023; accepted 24 July 2023

Abstract: The morphology, chemical composition, mechanical properties of the interface reaction products and their effects on the shear strength of the Au−Ge/Cu soldering joint were systematically investigated. The results showed that a close-packed hexagonal (HCP) structure solid solution phase was formed at the interface after soldering at 400 °C for 5−60 min. The composition of the HCP phase varied among 78−46 at.% Cu, 9−42 at.% Au and ~12 at.% Ge. The Young's modulus and hardness of HCP phase were 105−112 GPa and 4.3−4.7 GPa, respectively. The shear strength of the 5 min soldering joint was 57 MPa; however, it increased to 68 MPa when the soldering time was prolonged to 60 min. The increasing shear strength can be ascribed to the formation of HCP ductile phase and its effect on depleting the brittle (Ge) phase. It suggested that a HCP structured solid solution formed at the interface could enhance the shear strength of the solder joint.

Key words: Au−Ge solder; interfacial reaction; solid solution; close-packed hexagonal structure; shear strength

1 Introduction

Soldering has been extensively utilized to form interconnections between the electronic components [1−4]. For decades, scientists and engineers have worked diligently to achieve high performance and reliability of soldering joints [5,6]. For instance, Sn-based [4,7] and Au-based [8,9] solders, with melting points of 180−280 °C, are designed to match the requirements of soldering joints for most electronic products. However, recently, high-frequency and high-power devices applied at high temperatures approximately 300 °C are becoming increasingly critical [10], which leads to enormous demands for high-temperature solder for electronic packages. The Au−28at.%Ge eutectic alloy consisting of (Au) and (Ge) phases, has a melting point of 361 °C [11,12]. It has favorable mechanical, thermal, and electrical performances, being an excellent candidate solder for use up to approximately 300 °C [12−14].

However, the mechanical properties of soldering joints and the reliability of electronic products are crucially determined by the interfacial reaction products between the solder and substrate [15−17]. Generally, the soldering joint presents excellent shear strength when the thin and uniform intermetallic compounds (IMCs) layer is formed at the interface [10,18−24]. For example, when the uniform Ni_2Ge and/or NiGe layer is formed at the Au−Ge/Ni soldering joint, the shear strength of the Au−Ge/Ni joint maintains at around 50 MPa [10,22,23]. The soldering joint will achieve a higher shear strength when a ductile multi-principal-element solid solution phase is formed

Corresponding author: Jian PENG, Tel/Fax: +86-731-88836638, E-mail: pengjianmse@csu.edu.cn
DOI: 10.1016/S1003-6326(23)66272-7

at the interface [22,24]. However, the formation of multi-principal-element solid solution reaction product requires the multiplication of principal elements of the substrate. It will dramatically increase the complexity of the soldering joint and soldering process, reducing the potential reliability of the soldering joint.

Cu is the most common substrate in electronic systems [15,25]. An interfacial reaction layer containing large amounts of Cu, Au, and Ge is commonly observed at the Au−Ge/Cu soldering joint. Nevertheless, it has no indistinct interface with either (Au) phase in Au−Ge solder or Cu substrate. In addition, this Cu−Au−Ge phase shows an extensive composition range [12,23,26]. Although it is reported as the ξ-$(Au,Cu)_5Ge$ phase roughly based on the chemical composition [12], the phase type, thickness, morphology of the reaction product, as well as its effects on the shear strength of the soldering joint are still unclear. This limits the application of Au−Ge-based solders and the design of Au−Ge solder joints in the advanced electronics industry.

Herein, the Cu substrate and Au−Ge eutectic solder were bonded at 400 °C for various durations. The close-packed hexagonal structure solid solution interfacial reaction product, designated as HCP, was found to form at the interface of the Au−Ge/Cu joints during the soldering process. The morphology, chemical composition, and mechanical properties of this HCP phase and their effects on the shear strength of the Au−Ge/Cu soldering joint were systematically investigated. This is critical for analyzing the interconnection between Au−Ge/Cu, which further helps to design Au−Ge solders and solder joints with outstanding mechanical performance.

2 Experimental

The Au−Ge eutectic solder lugs, with dimensions of 3 mm × 5 mm × 25 μm, from Beijing Nonferrous Metals and Rare Earth Research Institute of China, were used in the present work. The cold-rolled Cu (>99.5 wt.%) sheet of 1.5 mm in thickness was cut into specimens with dimensions of 33 mm × 5 mm × 1.5 mm. Before being used as the substrates, the obtained Cu specimens were mechanically polished, then cleaned with acetone in an ultrasonic washer for 5 min. The Au−Ge solder lug was placed into two Cu substrates, fixed with Teflon tape to prepare the Au−Ge/Cu solder joint. Finally, the Au−Ge/Cu joint was bonded in a furnace (under H_2 atmosphere) at 400 °C for 5, 20, and 60 min, respectively.

A RGM4100 universal mechanical machine was used to measure the shear strength of the solder joints, which operated at room temperature with a tensile rate of 1 mm/min. The average shear strength of each joint was based on at least three independent measurements. A Shimadzu XRD−6000 X-ray diffraction (XRD) instrument with a tube voltage of 35 kV and a current of 200 mA was used to measure the fractured surface of the joints to obtain the phase constitution. The scanning rate and angle range were set as 2 (°)/min and 20°−90°, respectively. After being mechanically ground and polished by an ion-beam polishing instrument (Leica EM TIC 3X), the cross-sections of the joints were characterized by a Tenscan Mira 3 scanning electronic microscope (SEM) equipped with electron backscattering diffraction (EBSD) detector and energy dispersive X-ray (EDX) detector. The scanning step and measured region for EBSD measurement were 60 nm and 25 μm × 25 μm, respectively. The crystal structure properties of the HCP phase used for EBSD measurement are listed in Table 1 [27]. An ultra-nanoindentation tester equipped with a Berkovich indenter (tip radius R≈50 nm) was used to measure the mechanical properties of the reaction products and solder matrix in solder joints.

3 Results

3.1 Morphology of interfacial reaction product layer

Figure 1(a) shows the joint after soldering at 400 °C for 5 min. The dark areas in the soldering region are the (Ge) grains with an average diameter

Table 1 Crystal structure properties of HCP phases [27]

Phase	Symbol	Pearson symbol	Space group number	a/nm	b/nm	c/nm	α/(°)	β/(°)	γ/(°)
HCP	$P6_3/mmc$	$hP2$	194	2.853	2.853	4.687	90	90	120

a, b and c are axial lengths; α, β and γ are interaxial angles

of (5.0±1.6) μm. Meanwhile, the bright matrix is the (Au) phase, in the backscattered electron (BSE) image. The Ge and Cu contents in this (Au) phase are about 7 at.% and 30 at.%, respectively, according to the EDX measurement. The grey region near the Cu substrate will be the interfacial reaction product. In combination with the XRD pattern from the fracture surface of the joint (Fig. 2(a)) and the Au−Ge−Cu phase diagram [28,29], the reaction product will be the HCP solid solution. The EBSD phase distribution (PD) map further verifies that the HCP layer in 5 min solder joint is a uniform layer, of about 1.8 μm in thickness, adjacent to the Cu substrate. (Fig. 3(a)). This HCP layer contains a large amount of Au, according to the element distribution maps (Fig. 3(a)) corresponding to Fig. 2(a). The EDX results for a representative location show that the chemical composition of the HCP is Cu−24Au−12Ge. It should be noted that the volume fraction of (Ge) in the solder matrix decreased from ~27.0 at.% in Au−Ge eutectic [22] to ~18.6 at.% after 5 min soldering since Cu dissolved in solder and HCP was formed at the interface.

When prolonging the soldering time from 5 to 20 min, the reaction product near the Cu substrate is still the HCP, according to the BSE image, XRD pattern and EBSD measurement, as illustrated in Figs. 1(b), 2(b) and 3(b), respectively. The EBSD PD map corresponding to the selected square region in Fig. 1(b) shows a uniform HCP layer near the Cu substrate (Fig. 3(b)). The thickness of this HCP layer increases from 1.8 to 5.6 μm when the soldering time increased from 5 to 20 min. The average grain size of HCP rises to 2.9 μm. In addition, the (Ge) content decreases from ~18.6 at.% to ~8.1 at.%, and the average grain size maintains at (5.7±3.1) μm. The depletion of (Ge) derives from two aspects. On the one hand, the formed HCP layer at the interface contains a constant 12 at.% Ge. On the other hand, the dissolved Cu in the (Au) phase enhances the Ge solubility in the (Au) matrix. As shown in Fig. 4, the Ge content in (Au) increases from 3 at.% in eutectic solder to 9 at.% in the solder joint.

The solder is almost depleted to form HCP solid solution after 60 min soldering. Only a few (Ge) particles, as low as 3.7 at.% of the total soldering region, scatter in the solder joint near the (Ge) particles, as illustrated in the BSE image (Fig. 1(c)). Their average grain size still maintains at (5.4±2.3) μm. The XRD diffraction peak from the (Au) phase is weaker than that from the HCP phase (Fig. 2(c)). The EBSD PD map of the selected square region near the substrate shows that HCP is the main phase in the soldering region, yet a few

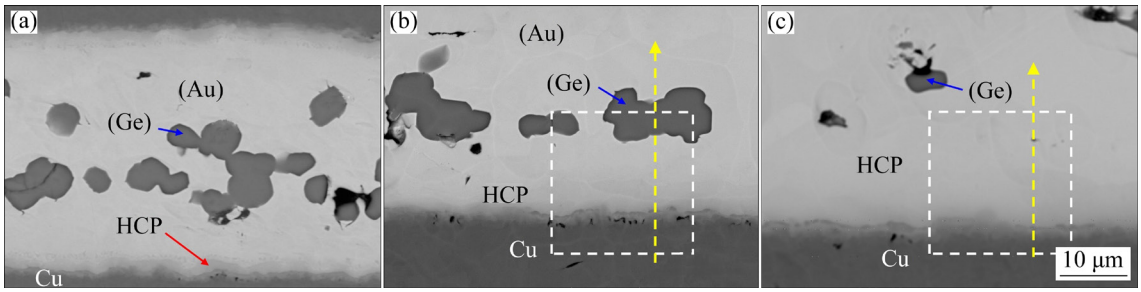

Fig. 1 BSE maps of Au−Ge/Cu joints after soldering for 5 min (a), 20 min (b), and 60 min (c)

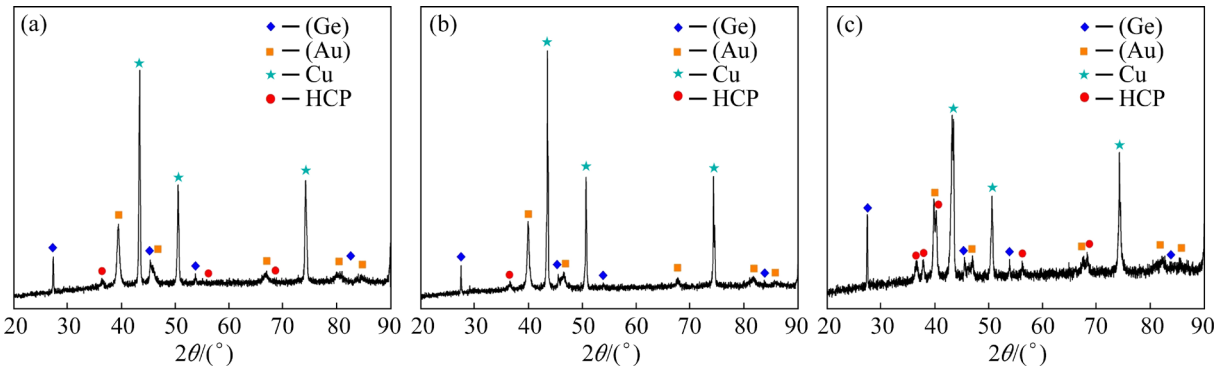

Fig. 2 XRD patterns of Au−Ge/Cu joints after soldering for 5 min (a), 20 min (b), and 60 min (c)

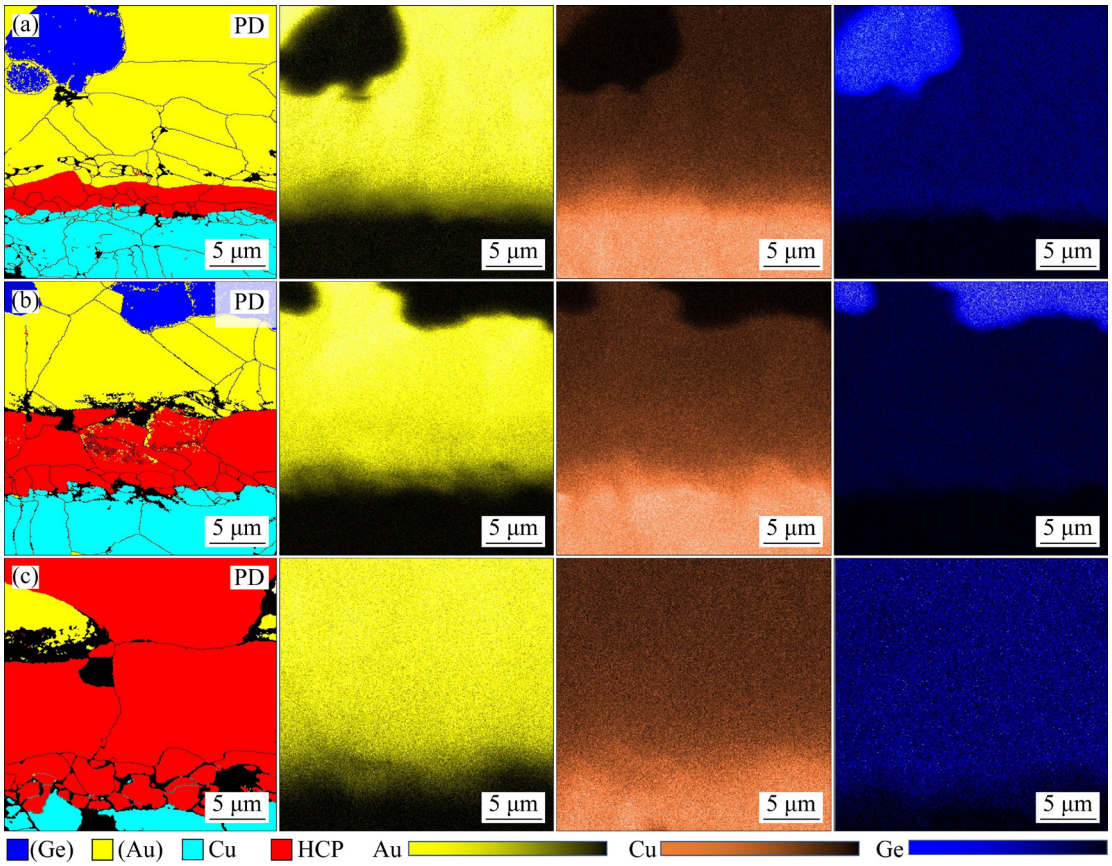

Fig. 3 EBSD phase distribution and EDS maps of Au−Ge/Cu joints after soldering for 5 min (a), 20 min (b), and 60 min (c)

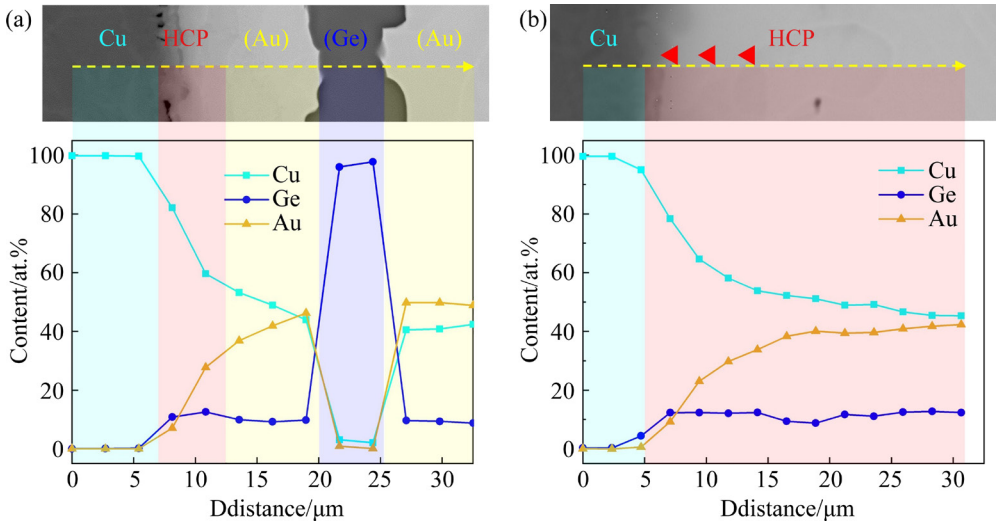

Fig. 4 Chemical composition profiles of Au−Ge/Cu joints after soldering for 20 min (a) and 60 min (b)

(Au) grains maintain in the middle of solder region (Fig. 3(c)). The HCP grains grow to 9.4 μm in average diameter. The bulky HCP grains are formed opposite to the Cu side, although the HCP grains adjacent to the Cu substrate are still small.

In brief, the HCP solid solution phase is formed at the Au−Ge/Cu interface after soldering at 400 °C for 5−60 min. The average grain size and layer thickness increase with prolonging soldering time. The Au−Ge eutectic solder is depleted to form the HCP phase during the soldering process, as shown in Reaction (1):

$$(Au)+(Ge)+Cu \rightarrow HCP \quad (1)$$

However, the HCP layer shows a composition gradient perpendicular to the interface, as illustrated in Fig. 4. Figure 4(a) presents the chemical composition profile towards the yellow arrow in the 20 min solder joint (Fig. 2(b)). The HCP phase formed adjacent to the Cu substrate shows high Cu (59−82 at.%) and Au (7−27 at.%) contents. Especially, the Ge content in HCP maintains at ~12 at.%, which is higher than that of ~9 at.% in the (Au) phase near the HCP layer. According to the Au−Ge phase diagram, the Ge content in the (Au) phase is 3 at.% [30]. However, the Cu was dissolved in (Au) to form a continuous solid solution, increasing the solubility of Ge in (Au) to ~9 at.% [29]. As shown in Fig. 4(a), the Cu content in the (Au) phase can even be as high as 53 at.%.

The (Au) phase in the solder joint is almost depleted to form the HCP layer after soldering for 60 min. The chemical composition profile of the product layer shows that the HCP consists of 78−46 at.% Cu, 9−42 at.% Au and ~12 at.% Ge (Fig. 4(b)). Similar to the 20 min solder joint, the HCP also suggests an obvious composition gradient perpendicular to the interface. This composition gradient is in contrast to the face-centered cubic structured product in the Au−Sn/CuNiAg solder joint. The face-centered cubic structured product at various locations of the joints soldered for various durations showed similar chemical composition, load (P)–depth (h) curves, and mechanical properties [31].

3.2 Mechanical properties of interfacial reaction products

Corresponding to the composition gradient, the HCP phase shows certain mechanical properties gradient. Figure 5 illustrates the indentations at the 60 min soldered Au−Ge/Cu joint and relevant P–h curves. The dark, red, and blue P–h curves respond to the A, B, and C indentations that are about 2, 5 and 8 μm from the Cu substrate, respectively. The hardness from A, B, and C indentations is 4.3, 4.4, and 4.5 GPa, respectively, as listed in Table 2. It indicates that the HCP phase near the Cu substrate, with a low Au content, presents low hardness. Similar to the hardness variation, the indentations show similar Young's modulus variation trend, which are 105, 107 and 112 GPa for A, B, and C indentations, accordingly.

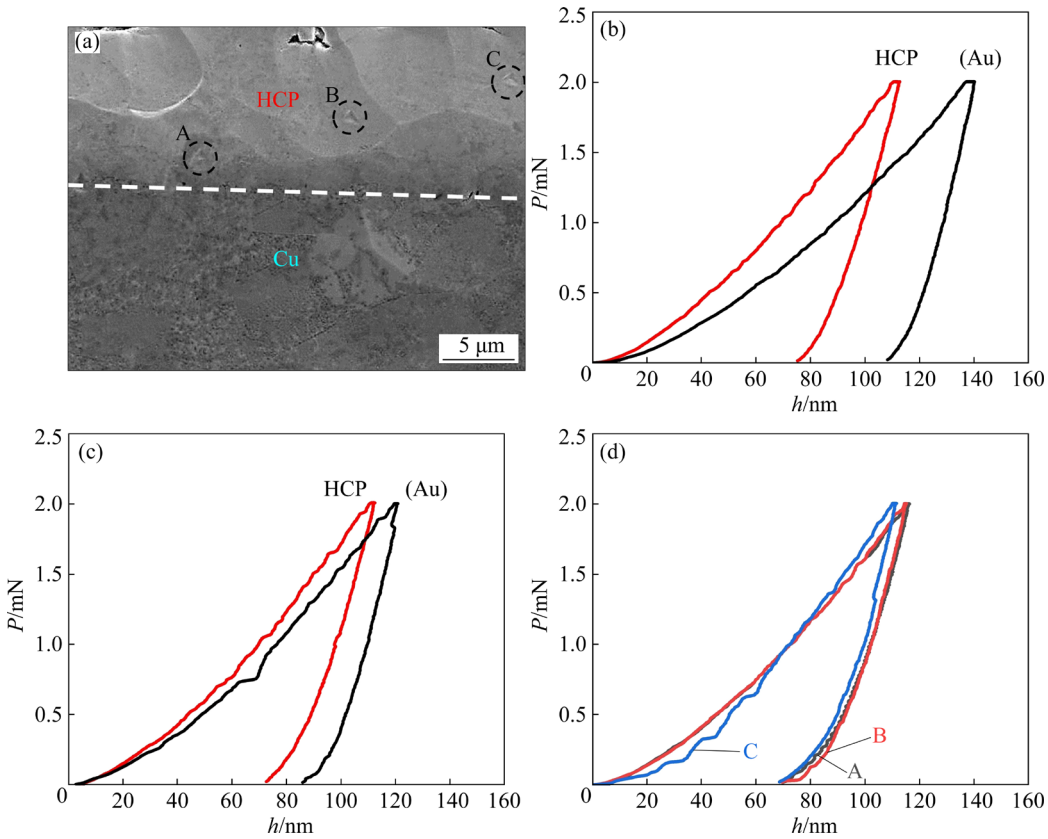

Fig. 5 Representation of indentations in 60 min solder joint (a) and representative P–h curves of indentations in joints after soldering for 5 min (b), 20 min (c), and 60 min (d)

Generally, the power law description (Eq. (2)) can be used to roughly illustrate the plastic deformation behavior of ductile alloys. Hence, a simple elastoplastic function was used to describe the true stress–true strain curve as follows.

$$\sigma=\begin{cases}E\varepsilon_{\mathrm{y}}, \text{ for } \sigma \le \sigma_{\mathrm{y}} \\ \sigma_{\mathrm{y}}\left(1+\dfrac{E}{\sigma_{\mathrm{y}}}\varepsilon_{\mathrm{p}}\right)^{n}, \text{ for } \sigma > \sigma_{\mathrm{y}}\end{cases} \tag{2}$$

where σ is the stress; E is Young's modulus; n is the strain hardening exponent; σ_{y} is the initial yield stress; ε_{y} is the corresponding yield strain; ε_{p} is the nonlinear part of the total effective strain accumulated beyond ε_{y}. The parameters of the representative $P-h$ responses, listed in Table 2, can be used to calculate the yield strength (σ_{y}) and strain hardening rate (n) by using the reverse analysis method [33]. In Table 2, C is loading curvature, $\mathrm{d}P_{\mathrm{u}}/\mathrm{d}h|_{h_{\mathrm{m}}}$ is the initial unloading slope, h_{r} is the residual indentation depth after unloading, h_{m} is the maximum indentation depth, and P_{m} is the maximum load. The estimated true stress–true strain curves of the phases are presented in Fig. 6.

According to the estimated true stress–true strain curves, in the joint after soldering for 60 min, the A indentation has a shear strength of 302 MPa and a strain hardening rate of 0.563. However, the B indentation, about 5 μm far away from the Cu substrate, presents shear strength of 386 MPa and a strain hardening rate of 0.532. The C indentation, with the highest Au content in all three indentations, shows the highest shear strength of 640 MPa, yet a strain hardening rate of 0.368. It indicates that the HCP with higher Au content shows a high shear strength but a low strain hardening rate.

The representative $P–h$ curves of the HCP phase in the 5 min and 20 min solder joints are shown in Figs. 5(a) and (b), respectively. The indentations in both 5 min and 20 min solder joints are about 2 μm away from the Cu substrate. Their Young's modulus and hardness are 103, 4.7 and 105, 4.7 GPa, respectively, as listed in Table 2. The estimated strain hardening rates from all three indentations are 0.550−0.565. Meanwhile, the estimated yield strengths are 302−424 MPa, as shown in Fig. 6(d). It indicates that HCP near the Cu substrate (about 2 μm) presents similar mechanical properties with the 60 min solder joint.

After the soldering process, the (Au) in the solder matrix shows Young's modulus of 97 GPa, which is lower than that of the HCP phase. In addition, the hardness of the (Au) is also lower than that of the HCP phase in soldering. In the 5 min solder joint, the Cu and Ge contents in the (Au) are about 30 at.% and 7 at.%, respectively. The hardness from nano-indentation is 3.1 GPa. In comparison, in the 20 min solder joint, the hardness of the (Au) phase is about 4.2 GPa, for the (Au) phase containing about 9 at.% Ge and above 40 at.% Cu. However, Young's modulus of (Au) in eutectic Au−Ge solder was reported as only 78 GPa [32]. The hardness and Young's modulus of (Au) phase are sensitive to the Cu and Ge contents. The dissolved Cu in the (Au) solder matrix during the soldering process, accompanied by the increased Ge solubility in (Au), increases the hardness of the (Au) phase. It should be noted that

Table 2 Parameters obtained from $P-h$ curves for (Au), HCP, and (Ge) phases

Soldering time/min	Phase	Young's modulus/GPa	Hardness/GPa	C/GPa	$(\mathrm{d}P_{\mathrm{u}}/\mathrm{d}h\|_{h_{\mathrm{m}}})$/(kN·m^{-1})	$h_{\mathrm{r}}/h_{\mathrm{m}}$	P_{m}/N
Au−Ge eutectic	(Au)	78 [32]	–	–	–	–	–
	(Ge)	103 [32]	–	–	–	–	–
5	HCP	103	4.7	84.4	75.2	0.773	0.002
	(Au)	97	3.1	63.1	88.9	0.844	0.002
20	HCP	105	4.7	84.3	74.8	0.776	0.002
	(Au)	97	4.2	76.2	72.1	0.788	0.002
	(Ge)	130	7.0	219	71.9	0.720	0.002
60	HCP (A)	105	4.3	78.8	79.0	0.794	0.002
	HCP (B)	107	4.4	82.7	85.1	0.794	0.002
	HCP (C)	112	4.5	85.2	75.0	0.819	0.002

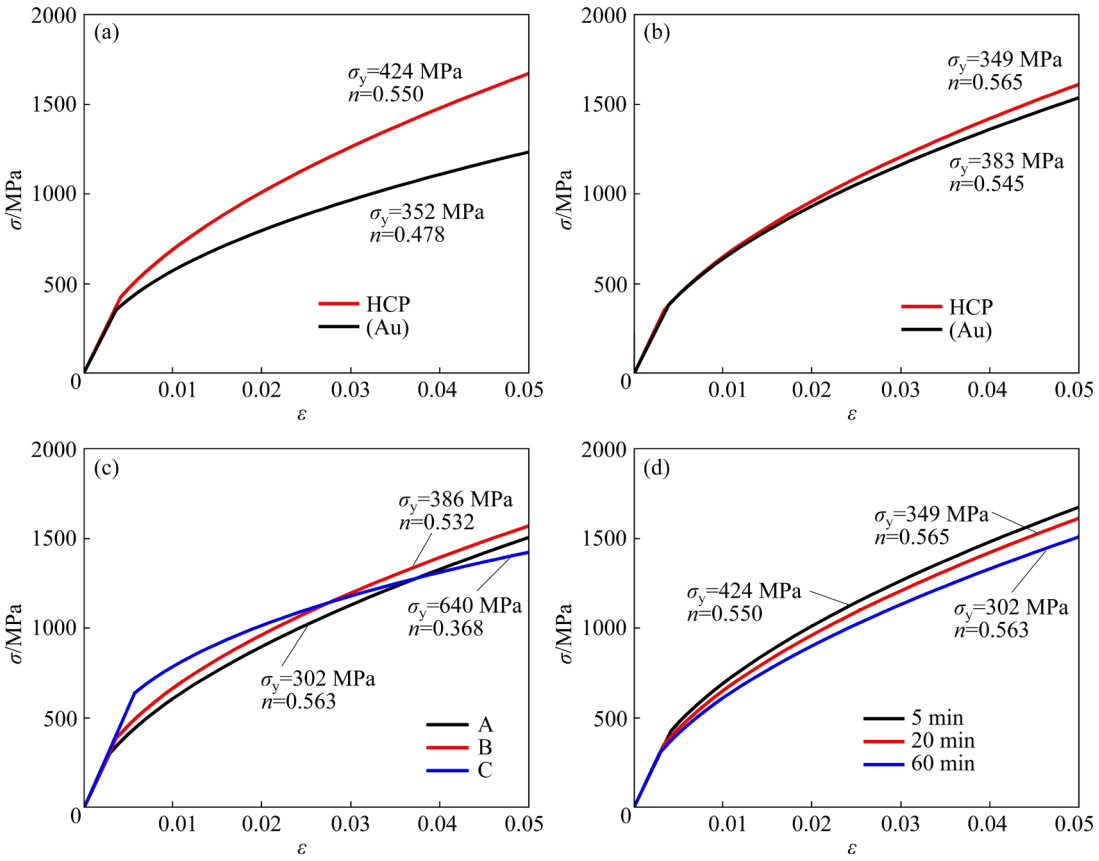

Fig. 6 Estimated true stress–true strain curves of phases in joints after soldering for 5 min (a), 20 min (b), 60 min (c), and comparison of HCP curves (d)

the (Ge) phase demonstrates a diamond-structure, which has a slight Au and Cu solution. Therefore, the (Ge) in all the joints was treated as a brittle phase with Young's modulus of 130 GPa.

3.3 Shear behavior of soldering joint

To clarify the effects of the HCP layer on enhancing the shear strength of the Au−Ge bonded joint, the solder joints were shear fractured at room temperature with a 1 mm/min tensile rate. Figure 7 shows the fractured surfaces of the joints. The fracture occurs predominantly along the fragmented bulk (Ge) grains in the solder matrix, showing a brittle fractured surface after soldering for 5 min. Interestingly, the crack along with the (Ge) grains is closest to the Cu substrate. The brittle nature of (Ge) responds to the cleavage fracture mechanism of the solder joint. The Au−Ge eutectic solder suggests brittle nature due to the high content of the brittle (Ge) phase [14]. Although the fracture still tends to develop along the (Ge) grains, the volume fraction of (Ge) in the solder joint decreases from 18.6 at.% to 8.1 at.% in 20 min solder joint. Therefore, the ductile fractured features can be observed in the joint after soldering for 20 min. In the case of the 60 min solder joint, the fracture shows ductile fracture. This clearly illustrates that prolonging soldering time is accompanied with the transformation from a cleavage fracture to a ductile fracture.

The shear strength evolution of the Au−Ge/Cu joints is illustrated in Fig. 8. The shear strength of the 5 min solder joint was 57 MPa, which increased to 62 MPa after soldering for 20 min. The highest shear strength of 68 MPa was achieved when the soldering time was increased to 60 min. Apparently, the shear strength of the Au−Ge/Cu joint increased with increasing soldering time from 5 to 60 min, which was higher than that of the Au−Ge/Cu−70Ni joints of 59 MPa [22] and Au−Ge/Ni joints of 50 MPa [23], of which the Ni−Ge intermetallic compounds (NiGe, Ni_2Ge and/or Ni_5Ge_3) were formed at the interface. The highest shear strength of the Au−Sn/Cu joint reached 69 MPa [34]. However, the brittle $Au_{6.6}Cu_{9.6}Sn_{3.8}$ phase were formed at the interface of Au−Sn/Cu solder joints;

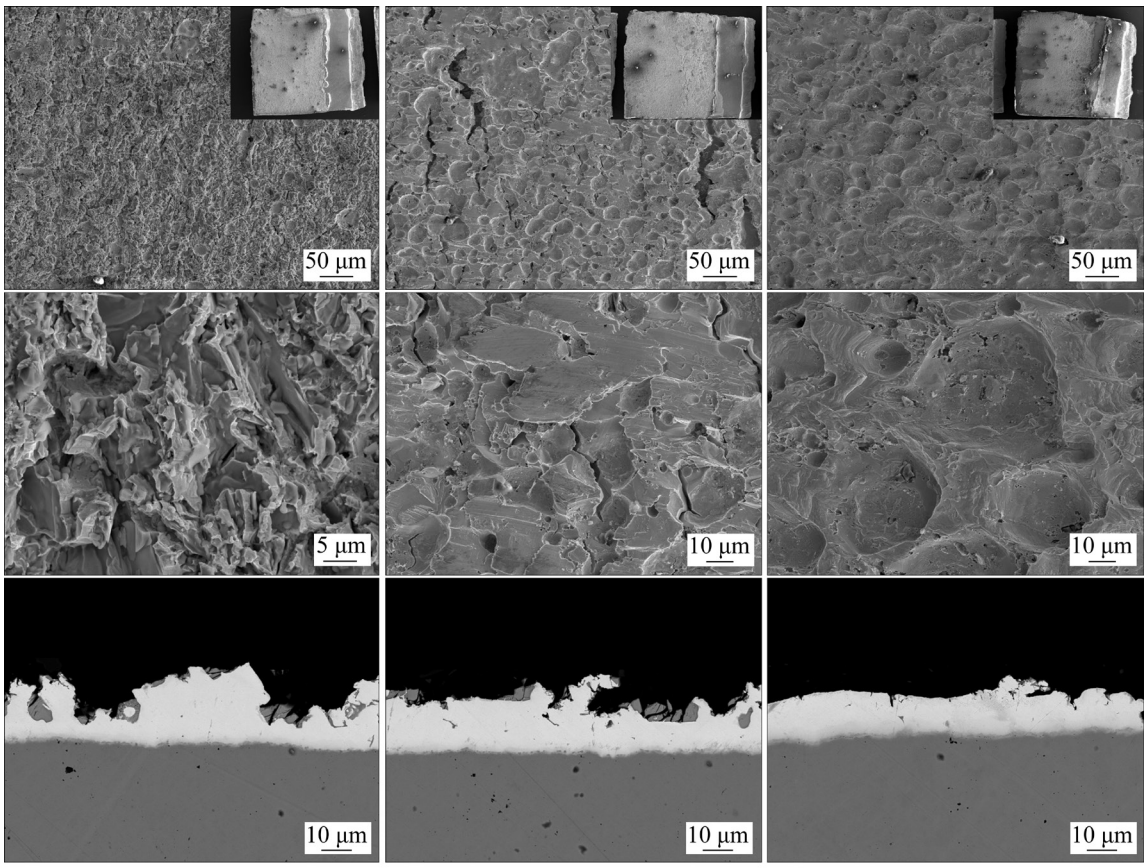

Fig. 7 Fracture morphologies of Au−Ge/Cu joints after soldering for 5 min (a), 20 min (b), and 60 min (c)

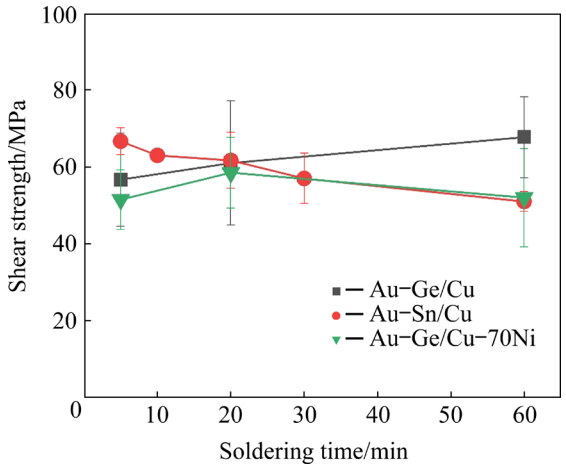

Fig. 8 Shear strength of Au−Ge/Cu, Au−Sn/Cu [34] and Au−Ge/Cu−70Ni [22] soldering joints

the grain boundaries of this IMC were fragile. Therefore, the Au−Sn/Cu joint was dominated by the intergranular fracture model, and their shear strength decreased with the prolonged soldering time [34]. This suggests that the shear strength of the Au−Ge/Cu joints benefits from the formation of the HCP phase.

4 Discussion

As mentioned above, the HCP layer was formed at the interface in the joint after soldering for 5−60 min. Figure 9 illustrates the interfacial reaction in Au−Ge/Cu joints. Formation of the HCP is accompanied by the depleted (Ge) and (Au) solder matrix, enhanced shear strength of the joint, as well as cleavage to ductile fracture transformation.

To determine the effects of HCP, the finite element (FE) models were employed to analyze the stress distribution in the joints by using ANSYS software (Fig. 10). The soldering region was set as 100 μm × 30 μm as simplification. The HCP was treated as a planer layer near the Cu substrate, and the (Ge) particles were treated as random distributing circles in the joint. The fraction, grain size, and grain size deviation of the (Ge) particles and thickness of the HCP layer from BSE and EBSD measurements were used to build the FE models. The estimated true stress−true strain curves

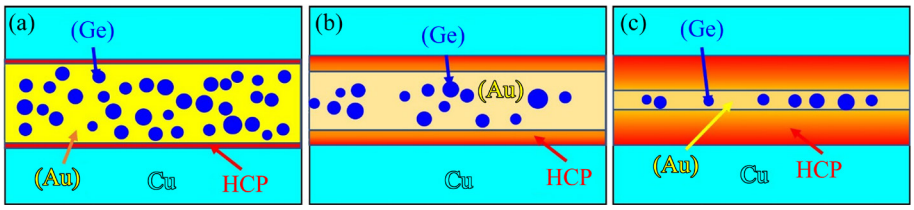

Fig. 9 Schematic diagrams showing interfacial reaction in Au−Ge/Cu joints after soldering for 5 min (a), 20 min (b), and 60 min (c)

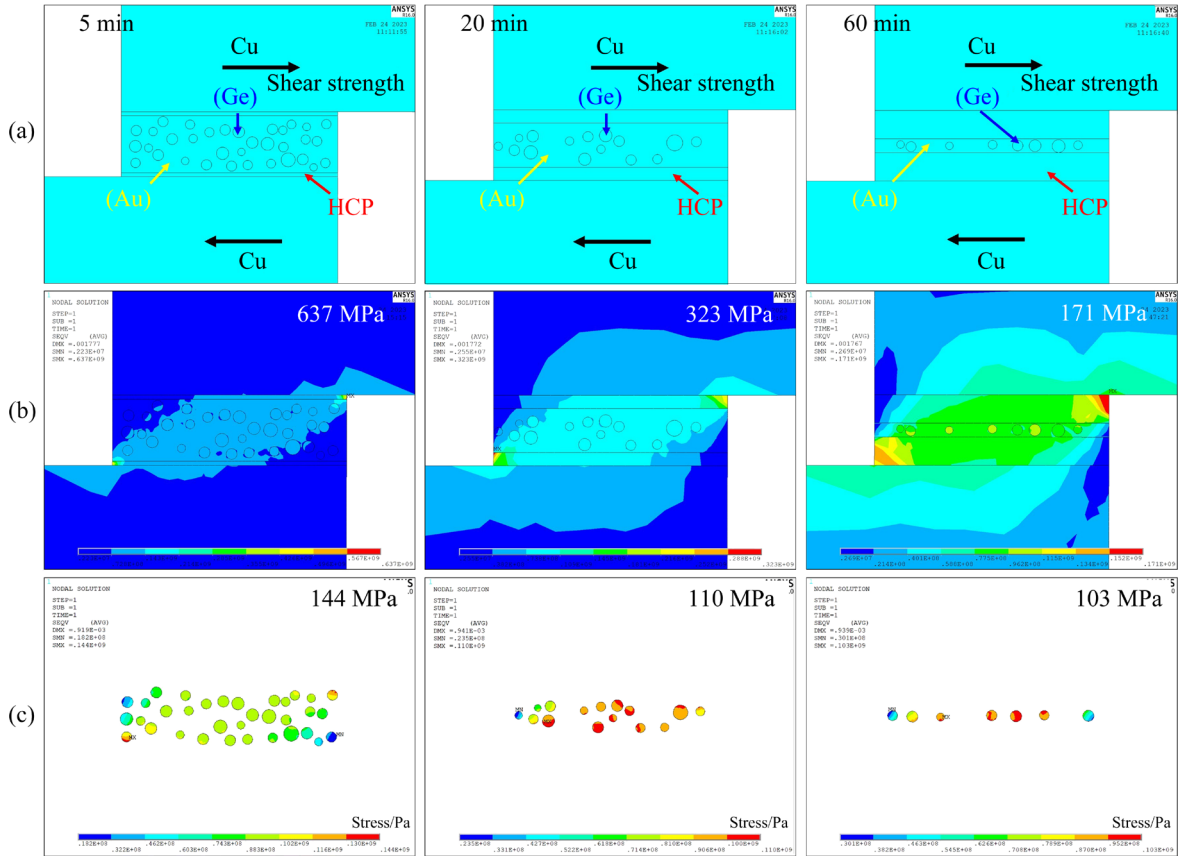

Fig. 10 Au−Ge/Cu joints after applying constant shear strength of 40 MPa: (a) Reacted interface in FE models; (b) Local stress concentration in HCP near substrate; (c) Equivalent plastic stress contour of bonded joints

from nanoindentations, as shown in Fig. 6, were used as the material properties for FE models.

The ductile HCP released a local strain concentration and changed the location and maximum value of the strain localization under shear stress (Fig. 10). After applying a constant shear strength of 40 MPa on the models, the maximum stress in the joint decreased with increasing thickness of the HCP layer. After bonding for 5 min, the thickness of the HCP layer was approximately 1.8 μm. The maximum stress in the bonded joint was 637 MPa, and the maximum equivalent plastic strain was observed in the HCP layer near the corner. However, the maximum stress decreased to 323 MPa when the thickness of the HCP layer increased to ~5.6 μm. It reached 171 MPa when the soldering time was increased to 60 min. Meanwhile, the maximum equivalent plastic strain appeared in the plastic HCP. The ductile reaction products have been frequently reported to release local strain concentration, and then enhance the shear strength of the soldering joint [22,24,31]. In the Au−Sn/Ni joint, only a brittle Ni_3Sn_2 phase layer was formed near the substrate, the maximum stress that appeared in the Ni_3Sn_2 layer was 1.5 GPa [35,36]. However, the maximum stress decreased to 546 MPa when a ductile layer of ~1 μm thickness was formed at the interface. The shear strength of the solder joint increased from 48 to 69 MPa [24,31].

The maximum stress of (Ge) decreased with increasing soldering time, although it was obviously lower than the stress in the HCP phase (Fig. 11(a)). The maximum stress of (Ge) in the 5 min solder joint, is 140 MPa, which is higher than that of 110 MPa in the 20 min solder joint as well as 103 MPa in the 60 min solder joint. As shown in Fig. 7, the fracture occurred along with the (Ge) grains since the brittle (Ge) would be broken under certain stress. Therefore, the joint with a lower maximum stress of (Ge) under a constant shear strength would suffer a high shear strength. The simulation results are consistent with the fact that the 60 min solder shows high shear strength.

It should also be noted that the mechanical property variations of the HCP only play tiny effects on the maximum stress of (Ge). The indentations A, B, and C in 60 min solder joint have different yield strengths and strain hardening rates as listed in Table 2. However, the calculated maximum stress of (Ge) is 103, 102, and 100 MPa after applying the true stress−true strain curves from A, B, and C indentations, respectively (Fig. 11(b)).

The minimum distance from the (Ge) grains to the substrate, instead of the volume fraction of (Ge), determines the maximum stress of the (Ge). Figure 11(c) illustrates the maximum stress of (Ge) versus the minimum distance from (Ge) to the substrate. The maximum stress of the (Ge) particles decreases from 144 to 113 MPa when the minimum distance from (Ge) to the substrate increases from 1.8 to 8 μm, even the content of (Ge) particles maintains at 18.6 at.%. In contrast, although the content of (Ge) is 3.7 at.% in 60 min joint, the maximum stress in (Ge) could increase up to 173 MPa when these (Ge) particles are 10 μm deviation from the central axis (Fig. 11(d)).

Thus, it can be concluded that the increased shear strength after prolonging soldering time will derive from the HCP formation. On the one hand, the ductile HCP layer was formed at the interface, releasing stress concentration in the joint. On the other hand, the brittle (Ge) particles, especially the particles near the substrate, were depleted during the formation of the HCP phase. Similar features can be found in the Au−Sn/Cu−Ni and Au−Ge/Cu−Ni joints [22,24,31]. The ductile layer formed

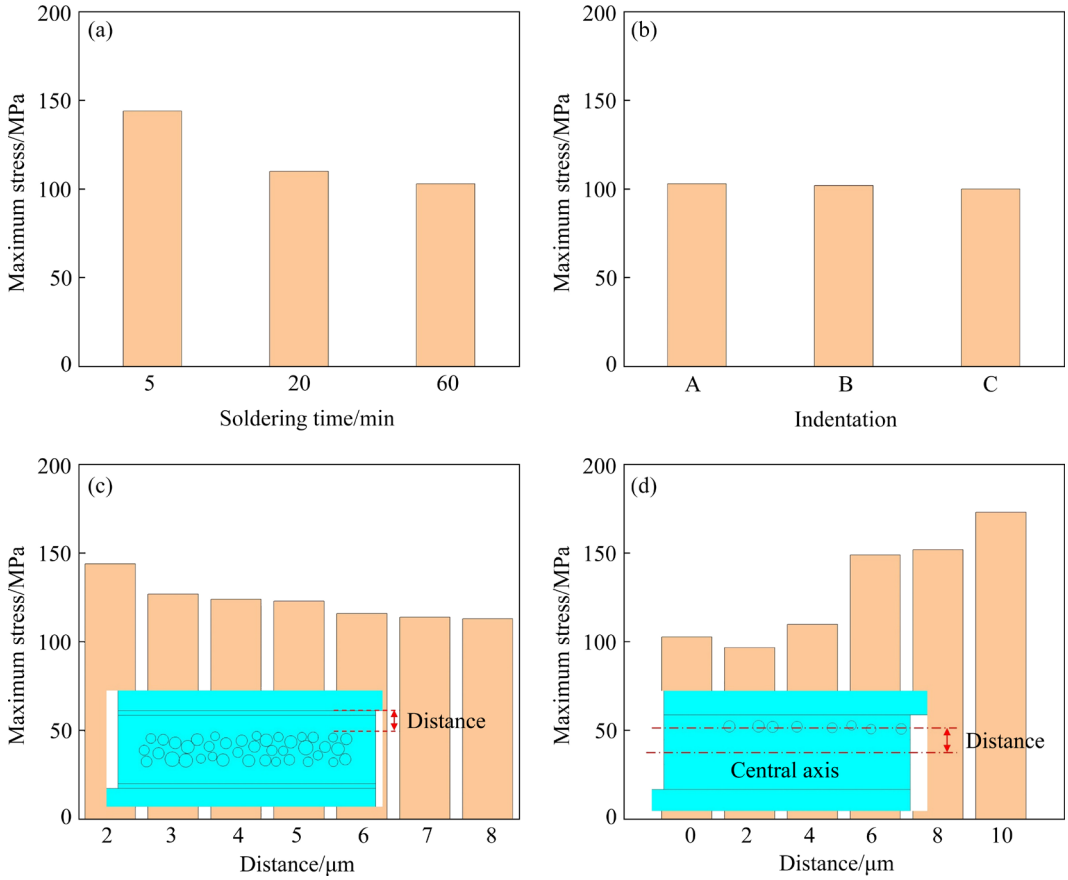

Fig. 11 Maximum local stress of (Ge) in joints: (a) Effect of soldering time; (b) Effect of mechanical properties of HCP; (c) Effect of minimum distance from (Ge) to substrate; (d) Effect of distance from (Ge) to central axis

near the substrate enhanced the shear strength of the joint. However, the formation of ductile phases in those joints is accompanied by brittle Ni_3Sn_2 particles. Hence, the shear strength of the joint will decrease when a large fraction of Ni_3Sn_2 particles are formed. In contrast, the depletion of the brittle phase accompanies with the formation of ductile HCP; therefore, the mechanical property of Au−Ge/Cu is enhanced with prolonging soldering duration. This also provides a guide for designing the Au−Ge-based solders and solder joints. For example, adding adequate alloying element, e.g. Sn, Sb [26] into Au−Ge eutectic solder can accelerate the depletion of Ge in the solder joint during the soldering process.

5 Conclusions

(1) The close-packed hexagonal structured HCP solid solution was formed in the Au−Ge/Cu joint after soldering at 400 °C for 5−60 min. The HCP layer has a constant Ge content of ~12 at.%, yet the Au content gradient is perpendicular to the interface. The range of this HCP solid solution is revealed as 78−46 at.% Cu, 9−42 at.% Au and ~12 at.% Ge.

(2) The HCP showed Young's modulus range of 105−112 GPa and hardness range of 4.3−4.7 GPa. The HCP phase adjacent to the Cu substrate, with low Au content, has lower Young's modulus and hardness. A representative estimated stress−strain curve for the HCP phase adjacent to the Cu substrate in 60 min solder joint shows a shear strength of 302 MPa and a strain hardening rate of 0.563.

(3) The shear strength of the joint was 57 MPa after soldering for 5 min, yet increased to 68 MPa when the soldering time was prolonged to 60 min. The HCP phase has ductile nature, especially, the HCP formation depletes the brittle (Ge) phase. Thus, the shear strength of the joint increases with increasing the HCP layer thickness.

Acknowledgments

The authors would like to acknowledge financial support from the Natural Science Foundation of Hunan Province, China (No. 2023JJ40473), and the National Science and Technology Project of China (No. 15452252).

References

[1] TU K N, LIU Y X. Recent advances on kinetic analysis of solder joint reactions in 3D IC packaging technology [J]. Materials Science and Engineering: R, 2019, 136: 1−12.

[2] MAO Yong, ZHU Dan-li, HE Jun-jie, DENG Chao, SUN Ying-jie, XUE Guang-jie, YU Heng-fei, WANG Chen. Hot deformation behavior and related microstructure evolution in Au−Sn eutectic multilayers [J]. Transactions of Nonferrous Metals Society of China, 2021, 31: 1700−1716.

[3] CHENG Shun-feng, HUANG Chien-ming, PECHT M. A review of lead-free solders for electronics applications [J]. Microelectronics Reliability, 2017, 75: 77−95.

[4] TAN X F, GU Q F, BERMINGHAM M, MCDONALD S D, NOGITA K. Systematic investigation of the effect of Ni concentration in Cu−*x*Ni/Sn couples for high temperature soldering [J]. Acta Materialia, 2022, 226: 117661.

[5] ZHANG Peng, XUE Song-bai, WANG Jian-hao. New challenges of miniaturization of electronic devices: Electromigration and thermomigration in lead-free solder joints [J]. Materials & Design, 2020, 192: 108726.

[6] LIU Y, PU L, YANG Y, HE Q, ZHOU Z, TAN C, ZHAO X, ZHANG Q, TU K N. A high-entropy alloy as very low melting point solder for advanced electronic packaging [J]. Materials Today Advances, 2020, 7: 100101.

[7] DURGA A, WOLLANTS P, MOELANS N. Phase-field study of IMC growth in Sn–Cu/Cu solder joints including elastoplastic effects [J]. Acta Materialia, 2020, 188: 241−258.

[8] PENG J, WANG R C, ZHU M X, LI Z M, LIU H S, MUKHERJEE A K, HU T. 2430% superplastic strain in a eutectic Au−Sn alloy with micrometer-sized grains maintained by spinodal-like decomposition [J]. Acta Materialia, 2022, 228: 117766.

[9] CHIDAMBARAM V, HALD J, HATTEL J. Development of gold based solder candidates for flip chip assembly [J]. Microelectronics Reliability, 2009, 49: 323−330.

[10] LIN S K, TSAI M Y, TSAI P C, HSU B H. Formation of alternating interfacial layers in Au−12Ge/Ni joints [J]. Scientific Reports, 2014, 4: 1−5.

[11] LARSSON A, AAMUNDTVEIT K E. On the microstructure of off-eutectic Au−Ge joints: A high-temperature joint [J]. Metallurgical and Materials Transactions A, 2020, 51: 740−749.

[12] LARSSON A, TOLLEFSEN T A, LØVVIK O M, AASMUNDTVEIT K E. A review of eutectic Au−Ge solder joints [J]. Metallurgical and Materials Transactions A, 2019, 50: 4632−4641.

[13] CHIDAMBARAM V, YEUNG H B, SHAN G. High reliability gold based solder alloys for micro-electronics packaging for high temperature applications [C]// Proceedings of the 19th IEEE International Symposium on the Physical and Failure Analysis of Integrated Circuits. Singapore, IEEE, 2012: 1−6.

[14] MSOLLI S, DALVERNY O, ALEXIS J, KARAMA M. Mechanical characterization of an Au−Ge solder alloy for high temperature electronic devices [C]//Proceedings of the 6th International Conference on Integrated Power Electronics Systems. Nuremberg, Germany, IEEE, 2010: 1−5.

[15] LAURILA T, VUORINEN V, KIVILAHTI J K. Interfacial reactions between lead-free solders and common base materials [J]. Materials Science and Engineering: R, 2005, 49: 1−60.

[16] SUN Yue, LIU Hua-shan, XIE Zhi-yun, JIN Zhan-peng. Prediction of interfacial reaction products between metals with same lattice structure through thermodynamic modeling [J]. Calphad, 2016, 52: 180−185.
[17] LEE B J, HWANG N M, LEE H M. Prediction of interface reaction products between Cu and various solder alloys by thermodynamic calculation [J]. Acta Materialia, 1997, 45: 1867−1874.
[18] CHU K M, SOHN Y, MOON C. A comparative study of Cn/Sn/Cu and Ni/Sn/Ni solder joints for low temperature stable transient liquid phase bonding [J]. Scripta Materialia, 2015, 109: 113−117.
[19] ATTARI V, GHOSH S, DUONG T, ARROYAVE R. On the interfacial phase growth and vacancy evolution during accelerated electromigration in Cu/Sn/Cu microjoints [J]. Acta Materialia, 2018, 160: 185−198.
[20] KE J H, CHUANG H Y, SHIH W L, KAO C R. Mechanism for serrated cathode dissolution in Cu/Sn/Cu interconnect under electron current stressing [J]. Acta Materialia, 2012, 60: 2082−2090.
[21] PARK M S, GIBBONS S L, ARRÓYAVE R. Phase-field simulations of intermetallic compound growth in Cu/Sn/Cu sandwich structure under transient liquid phase bonding conditions [J]. Acta Materialia, 2012, 60: 6278−6287.
[22] WANG Meng, LIU Hua-shan, PENG Jian. Enhancing the shear strength of the Au–Ge solder joint via forming a ductile face-centered cubic solid solution layer at the interface [J]. Journal of Materials Research and Technology, 2022, 19: 605−616.
[23] LEINENBACH C, VALENZA F, GIURANNO D, ELSENER H R, JIN S, NOVAKOVIC R. Wetting and soldering behavior of eutectic Au−Ge alloy on Cu and Ni substrates [J]. Journal of Electronic Materials, 2011, 40: 1533−1541.
[24] PENG Jian, WANG Meng, SADEGHI B, WANG Ri-chu, LIU Hua-shan, CAVALIERE P. Increasing shear strength of Au−Sn bonded joint through nano-grained interfacial reaction products [J]. Journal of Materials Science, 2021, 56: 7050−7062.
[25] DAEUMER M, SANDOVAL E D, AZIZI A, BAGHERI M H, BAE I J, PANTA S, KOULAKOVA E A, COTTS E, ARVIN C L, KOLMOGOROV A N, SCHIFFRES S N. Orientation-dependent transport properties of Cu_3Sn [J]. Acta Materialia, 2022, 227: 117671.
[26] WEYRICH N, JIN S, DUARTE L I, LEINENBACH C. Joining of Cu, Ni, and Ti using Au−Ge-based high-temperature solder alloys [J]. Journal of Materials Engineering and Performance, 2014, 23: 1585−1592.
[27] KING H W, MASSALSKI T B, ISAACS L L. Axial ratio changes in H.C.P. ζ phases in the systems Au−In−Cu and Cu−Ge−Au [J]. Acta Metallurgica, 1963, 11: 1355−1361.
[28] WANG J, JIN S, LEINENBACH C, JACOT A. Thermodynamic assessment of the Cu−Ge binary system [J]. Journal of Alloys and Compounds, 2010, 504: 159−165.
[29] JIN S, DUARTE L I, LEINENBACH C. Experimental study and thermodynamic description of the Au−Cu−Ge system [J]. Journal of Alloys and Compounds, 2014, 588: 7−16.
[30] OKAMOTO H, MASSALSKI T B. The Au−Ge (gold−germanium) system [J]. Bulletin of Alloy Phase Diagrams, 1984, 5: 601−610.
[31] PENG Jian, LIU Hua-shan, FU Li-ming, SHAN Ai-dang. Multi-principal-element products enhancing Au−Sn-bonded joints [J]. Journal of Alloys and Compounds, 2021, 852: 157015.
[32] NISHIYAMA T, OGAWA T, SAKAMOTO H. Evaluation of mechanical properties and nano-structure analysis of Au−20Sn and Au−12Ge solders [J]. Journal of the Society of Materials Science, Japan, 2007, 56: 913−919.
[33] DAO M, CHOLLACOOP N, VLIET K J V, VENKATESH T A, SURESH S. Computational modeling of the forward and reverse problems in instrumented sharp indentation [J]. Acta Materialia, 2001, 49: 3899−3918.
[34] PENG Jian, LIU Hua-shan, MA Hui-bin, SHI Xiu-mei, WANG Ri-chu. Microstructure evolution and mechanical reliability of Cu/Au−Sn/Cu joints during transient liquid phase bonding [J]. Journal of Materials Science, 2018, 53: 9287−9296.
[35] WANG Meng, LIU Hua-shan, WANG Ri-chu, PENG Jian. Thermally stable Ni/Au−Sn/Ni joint fabricated via transient liquid-phase bonding [J]. Materials Science and Engineering: A, 2020, 773: 138738.
[36] ZHU Z X, LI C C, LIAO L L, LIU C K, KAO C R. Au–Sn bonding material for the assembly of power integrated circuit module [J]. Journal of Alloys and Compounds, 2016, 671: 340−345.

界面密排六方固溶体提高 Au−Ge/Cu 焊点的剪切强度

王 檬[1,2]，彭 健[1]

1. 中南大学 材料科学与工程学院，长沙 410083；
2. Aragón Nanoscience and Materials Institute (CSIC–University of Zaragoza) and Condensed Matter Physics Department, C/Pedro Cerbuna 12, 50009 Zaragoza, Spain

摘 要：系统研究界面产物形貌、化学成分、力学性能及其对 Au−Ge/Cu 焊点剪切强度的影响。结果表明，在 400 ℃下钎焊 5~60 min 后，焊点界面生成密排六方结构固溶体相(HCP)。该 HCP 相成分为 78%~46% Cu, 9%~42% Au 和 ~12% Ge(摩尔分数)，杨氏模量为 105~112 GPa，硬度为 4.3~4.7 GPa。钎焊 5 min 焊点的剪切强度为 57 MPa，但钎焊 60 min 后焊点的剪切强度上升至 68 MPa。焊点强度的提高可归因于塑性 HCP 相的生成及其对脆性(Ge)相的消耗。这说明生成塑性 HCP 界面产物是一种能有效提高钎焊焊点剪切强度的方法。

关键词：金锗焊料；界面反应；固溶体；密排六方结构；剪切强度

(Edited by Wei-ping CHEN)